Photoreforming of model carbohydrate mixtures from pulping industry wastewaters

Francesco Conte[a], Gabriele Casalini[a], Laura Prati[a], Gianguido Ramis[b] and Ilenia Rossetti[a,*]

[a] Chemical Plants and Industrial Chemistry Group, Dip. Chimica, Università degli Studi di Milano, CNR-SCITEC and INSTM Unit Milano-Università, via C. Golgi 19, 20133 Milano, Italy

[b] Dip. Ing. Chimica, Civile ed Ambientale, Università degli Studi di Genova and INSTM Unit Genova, via all'Opera Pia 15A, Genoa, Italy

ABSTRACT

The photoreforming of organic molecules is a growingly interesting technology to achieve faster hydrogen production than with water splitting, while simultaneously mineralising organic pollutants in water. This paper investigates the possibility to produce hydrogen or gaseous fuel mixtures by using simulated wastewaters of the pulping industry. Glucose was first used as model molecule for carbohydrate-containing wastewaters, while tartaric acid was the model for those rich of carboxylic acids. Different titania catalysts were prepared starting form the P25 commercial material and monometallic Pt or Au, or bi-metallic Au_xPt_y formulations were prepared in form of surface-decorated nanomaterials.

The effect of pH and co-catalysts addition was explored, achieving after 5 h of irradiation the highest glucose conversion (15.2%) and H_2 productivity (4.1 mol H_2 kg_{cat}^{-1} h_{irr}^{-1}) with sample 1.0 wt%Au_6Pt_4/P25. This result competes with the best ones reported in the literature. Testing of tartaric acid showed much faster conversion of the substrate, but limited hydrogen productivity, ethane and

* Corresponding author: Fax +390250314300; email: ilenia.rossetti@unimi.it

CO_2 being the main products, anyway leading to a valorisable gaseous fuel mixture.

The best performing materials were also tested for the photoreforming of simulated wastewaters representative of pulping industry effluents, according to the two pulp processing technologies, the Kraft and sulphite ones. Similar results than tartaric acid were obtained when testing the Kraft spent liquor, mainly composed of hydroxycarboxylic acids. By contrast, the Sulphite spent liquor was mainly composed of carbohydrates, acetic and gluconic acids and led to methane as main product, possibly coming from the decarboxylation of acetic acid.

The results overall testify the interest of photoreforming to valorise wastewaters into gaseous fuels in a circular economy concept.

Keywords: Photoreforming; Photocatalytic hydrogen production; Glucose conversion; Pulping spent liquors; Wastewater treatment.

1. Introduction

The annual worldwide production of paper products stands around 410 Mton/year; Europe produces ca. 94 Mton/year, of which 41.8 Mton/year derived from cellulose pulp processing[1]. Italy is actually the 3rd country of Europe for paper production and the 10th or 9th on worldwide scale, with an annual production of 9 Mton/year and an internal market demand of 10.3 Mton/year. 50% of the raw materials exploited for producing paper is wastepaper, 15 % are inorganic filler and 35% is composed of cellulose pulp, extracted from wood. Italy produces by its own only the 9% of cellulose pulp that it needs, the remaining is imported [1].

Cellulose pulp can be obtained from wood by chemical, mechanical and chemo-mechanical processing, to separate lignin and part of hemicellulose from cellulose, according to the final application. Chemical processes are based on reactive leaching and are mainly two: the Kraft (alkaline sulfate process, predominant) and the sulphite one, the latter accounting for ca. 6% of the market [2]. The Kraft process returns fibers with better mechanical properties and it has become less

environmentally concerning and costly. On the other hand, the sulfite process is more flexible, both in terms of the variety of incoming raw material, of process conditions and of tuning of the properties of the pulp produced. Most sulphite plants expanded their business to fine chemicals, especially bio-surfactants derived from lignosulfonates, as well as the lignosulfonates themselves, recoverable from the spent liquors of wood cooking.

Also starting from these valuable revamps, from the beginning of the XXI century the entire pulp and paper industry has manifested a growing interest in diversifying its product portfolio by utilisation of side or waste streams, thereby creating new value chains.

The practice of spent liquors disposal (spent inorganic reactants and a variety of organic by-products and side products) is the following: after some obliged separations such as filtration of solid ashes and flotation/skimming of oil, they are concentrated to slurry passing from 15% wt of residual solid content to 65-70% wt. Such viscous slurry is often burned in a recovery boiler, which is designed both to completely oxidize to gaseous oxides all the organic compounds and to work as a steam-based power plant, supplying electricity. Spent inorganic reactants are regenerated with very high yield during burning, so they are collected and recycled to the wood pulping/cooking reactor or autoclave, limiting reactants make-up [1]. Wastewater effluents recovered from the condensate of the evaporation section contains only water, acetic acid, formic acid, low quantity of C3 acids and furfural.

The majority of the organic material in sulfite spent liquors originates from lignin (lignosulfonates) and hemicellulose (mainly low molecular weight carbohydrates). The heat value of lignosulfonates as fuel is rather high, roughly half of that of oil, whereas the one of the carbohydrate fraction is much lower, roughly only one-third of that of oil.

Black Kraft liquor is a very complex matrix containing a variety of products, and studies about further isolation of the products of carbohydrates degradation have been conducted up to the pilot scale since 1991.

Photoreforming is a possible green alternative to give value to processed liquors at train of

separation's end, which are rich in sugars for the sulphite process and in carboxylic hydroxy acids for the Kraft process [3–10]. It consists in photocatalytic water splitting assisted by organic molecules, which act as hole scavengers (HS), being oxidized more quickly than water. They prompt the electron-hole separation under illumination, consuming the holes faster than water oxidation, indirectly improving the hydrogen evolution reaction. The use of glucose is demonstrated for this application [11] and perfectly fits the logic of valorisation of the pulp industry residues, accomplishing both the functions of advanced oxidation treatment and smart waste valorization, producing H_2 in a circular way [12,13]. Photoreforming involves a lower Gibbs free energy than water splitting because the product of the short circuit oxidation half reaction is CO_2 instead of O_2 [14]. Photogenerated holes would also oxidize a sugar molecule faster than water, since water oxidation needs multielectron transfer to achieve stable products or intermediates.

The half reaction of H_2 production and the total sugar photoreforming are:

$$2\,H^+ + 2\,e^- \rightarrow H_2 \tag{1}$$

$$C_xH_yO_z + (2x - z)H_2O \rightarrow \left(2x - z + {}^{y}/_{2}\right)H_2 + x\,CO_2 \tag{2}$$

TiO_2 photocatalysts are the most widely reported for this application, whose features can be improved through the addition of co-catalysts, either metals or oxides with lower band gap [4].

Despite the attention devoted to photocatalytic hydrogen production, the use of complex substrates, simulating real industrial waste solutions, is rarely considered. Furthermore, the effect of the organic compounds in water acting as holes scavengers is not fully explored in the literature, especially they are not correlated to the pH and to the presence of co-catalysts.

This work intends to demonstrate the possibility to apply photoreforming to both the valorization of pulp and paper industry wastewaters and the exploitation of cellulosic hydrolysates from biomass, which lead to carbohydrate rich wastewaters. An advanced oxidation waste treatment is proposed, capable of co-generating H_2 and smaller quantities of simpler fuel chemicals in the gas phase while increasing the biodegradability index (BOD_5/COD) for correct wastewater disposal. Specific aims of this work are as follows. a) Glucose has been selected as model molecule for photocatalysts screening,

so that the best catalysts and conditions have been later applied to simulated pulping spent liquors. A discussion on the effect of pH, considering kinetic and thermodynamic effects related to band potentials is provided. b) Different materials have been compared. Surface decorated TiO_2-based materials have been prepared through different methods, such as wet impregnation, incipient wetness impregnation and complex-assisted precipitation. Commercial P25 titania has been added with Pt or Au as monometallic co-catalysts or in Au_xPt_y formulation. The materials were compared as for their optical, structural and textural properties, and tested for the photoreforming of glucose. c) The best performing materials and conditions have been applied for the photoreforming of tartaric acid as model compound for pulp processing leading to carboxylic acids mixtures. d) Finally, simulated wastewaters from the Kraft and sulphite pulp processing were tested to assess photoreforming of complex carbohydrate and carboxylic acid mixtures.

2. Experimental

2.1 Catalysts preparation

All the catalysts tested were based on TiO_2-P25 and differently surface decorated. Evonik P25 TiO_2 aeroxide is a nanometre-sized particulate material with a surface area of ca. 49 m^2/g and a typical anatase/rutile ratio of ca. 80:20, slightly changing with possible presence of max. 8% of an amorphous phase, because of batch-to-batch differences.

Metal loaded catalysts were investigated, based on a previous screening by our group for glucose photoreforming activity [15–17]. The composition of the tested catalysts is reported in Table 1.

Table 1: Samples composition and preparation procedures.

Sample	***Loading method***	***Content (wt%)***	***Notes***

P25	Bare	/	/
0.36 wt%Au/P25	Impregnation	0.36 wt% Au	H_2 activated, 3h, TPR T
0.36 wt%Pt/P25	Impregnation	0.36 wt% Pt	H_2 activated, 3h, TPR T
1.0 wt%Au/P25	Impregnation	1.0 wt% Au	Air calcined, 1h 400°C
1.0 wt%Pt/P25	Impregnation	1.0 wt% Pt	Air calcined, 1h 400°C
1.0 wt%Au_6Pt_4/P25	Sol Immobilisation	0.61 wt% Au + 0.39 wt% Au:Pt = 6:4 mol/mol	
1.0 wt%Au_8Pt_2/P25	Sol Immobilisation	0.79 wt% Au + 0.21 wt% Au:Pt = 8:2 mol/mol	

Single metal loading was done by impregnation (I) [18,19], using MilliQ water added with proper amounts of $AuCl_3$ or Pt acetylacetonate in a quantity sufficient to cover the powder. A suspension is formed after agitation thanks to a magnetic stirrer (2 hours). After that, water was removed via evaporation under reduced pressure. The recovered powder was left in oven (80 °C) overnight and then reduced in a tubular oven by heating (5 °C/min) up to 300°C for Au, 700°C for Pt in pure H_2 flow, according to a preliminary Temperature Programmed Reduction (TPR).

Sol immobilization (SI) [20,21] was employed for the synthesis of the two Au_xPt_y bimetallic catalysts. Firstly Au/TiO_2 was prepared by adding solid $NaAuCl_4 \cdot 2H_2O$ and a PVA solution (Au/PVA 1:0.5, w/w) to 100 mL of water. After 3 min, $NaBH_4$ (Au/$NaBH_4$ 1:4 mol/mol) was added to the previous solution under vigorous stirring. A ruby red Au^0 sol formed immediately. After few minutes, the colloid (acidified at pH 2 by H_2SO_4) was immobilized by adding the support (TiO_2, Evonik P25). The catalysts were filtered, washed and dried at 80°C for 4 hours. The so synthesised Au/TiO_2 powder was re-dispersed in 100 mL of water and added with solutions of Na_2PtCl_6 and PVA. H_2 was bubbled (50 mL/min) under atmospheric pressure and at room temperature into the suspension. After 2 hours, the slurry was filtered and the catalyst was washed several times with distilled water, then filtered

and dried.

2.2 Catalysts characterisation

X-Ray Powder Diffraction (XRPD) was used for the determination of crystalline phases using a Philips 3020 diffractometer and the crystal size was determined from the Scherrer equation.

Specific Surface Area (SSA) and porosimetry were determined by N_2 adsorption/desorption with an ASAP 2020-Micrometrics instrument, after outgassing for 4h at 150°C.

Diffuse Reflectance–UV/Vis spectroscopy (DR-UV-Vis) spectra were collected on a Cary 5000 UV-Vis-NIR spectrophotometer (Varian instruments) in the range of 200–900 nm and elaborated with a Tauc plot to determine the band gap of the materials.

2.3 Activity testing

All reagents were supplied by Sigma Aldrich: glucose (anhydrous, pur. 96%), sodium sulfate (anhydrous, pur. >99%), sodium perclorate (pur. >98%); L-(+)-arabinose (pur. >98%), D-(+)-xylose (pur. >99%), D-gluconic acid (solution, 50% wt in H_2O), acetic acid (glacial, pur. >99,7%), levulinic acid (pur. >97%), L-(+)-tartaric acid (pur. >99,5%), D-(-)-lactic acid (pur. >90%), glycolic acid (solution, 70% wt in H_2O), D-xylono-1,4-lactone (pur. >95%).

A batch bench scale plant was used, able to operate up to 20 bar, made of AISI 316 stainless steel, with net capacity of 1.3 L [22–24]. The outer jacket was connected to a heating/cooling bath and the inner temperature measured by a thermocouple. The reaction mixture was stirred by means of a magnetic stirrer placed below the reactor and N_2 was used for degassing and pressurizing at 4 bar.

UV light irradiation was provided by a medium pressure 125 W mercury vapour lamp with two bulbs, with maximum emission at 364 nm. Its radiant power was checked every 80h of operation using a photoradiometer (Delta OHM HD2102.2 equipped with LP 471A-UVeff probe), sensitive in the range 250-400 nm and resulted in average 153 W/m^2.

The best operating conditions have been determined in a previous research [19]: 80°C, 4 bar of N_2,

inert atmosphere, 5 g/L of hole scavenger (e.g. glucose), photocatalyst concentration 0.25 g/L. pH was always kept as naturally established, except when exploring the effect of pH, to avoid the need of correction in industrial operation and stirring was kept at 500 rpm.

Pulping spent liquors were simulated as carboxylic acids rich wastewaters (from spent black Kraft liquors) and sugars rich ones (from sulfite plant spent liquors). Best operative conditions of temperature, pressure and stirring were maintained. However, total hole scavenger concentrations were increased to 15 g/L to better represent the actual concentration reachable by such spent liquors [1].

A simulated wastewater formulation was defined as follows for processed spent liquors from birch sulfite cooking [2] (Table 2). In Part A masses are intended as kg of chemical composing the liquor produced for each ton of pulp. It has the same meaning in Part B-Liquor modelling, but they are modified or redefined according to the model molecule selected. Mass fractions of modelled liquor are obtained as percentage of the ratio among the kg produced for each model chemical to the total mass of chemical produced. Such obtained mass fractions (ω) are multiplied by the total hole scavenger mass desired defining the simulated wastewater formulation.

Table 2: Sulfite spent liquor chemical model. Part A is reprinted from [2].

Part A		Part B			
Real liquor composition		Liquor modeling		Representative solution	
Chemical - sugars	$m_{real\ prod}$ /kg	Model chemical	$m_{model\ prod}$ /kg	ω	$m_{chemical}$ /g
arabinose	10	arabinose	10	0.027	0.50
xylose	60	xylose	60	0.163	2.94
mannose	120	glucose	210	0.565	10.00
glucose	40				
galactose	50				
aldonic acids	50	gluconic acid	50	0.135	2.50
acetic acid	40	acetic acid	40	0.11	2.00
Total	370	Total	370	1	18.00

Mannose and galactose are epimers of glucose, so for our purposes they can be chemically represented by it. Aldonic acids fraction was modelized as gluconic one. 18 g are defined as total hole scavenger mass to obtain 15 g/L of total hole scavenger solution concentration.

The processed black liquor from birch Kraft cooking [2] is approximately described in Table 3. Operation to be done are the same as just described for the sulfite case, but many components (e.g. glucoisosaccarinic, 3-deoxypentonic, 3,4-dideoxypentonic, 2-hydroxybutanoic and xyloisosaccarinic acids) were unavailable on the market. Maximum similitude criterion was followed exploiting available chemicals: glucoisosaccarinic and xyloisosaccarinic acids were substituted by gluconic and xylonic acids, which carry one more -OH group on saturated 3-carbon. Their carboxylic groups are at the end of a linear carbon chain instead of the branched position on 2-carbon. It can undergo lactonization in acid environment. By virtue of that, xylonic acid was actually added as D-xylono-1,4-lactone; hydroxy-pentonic acids were not replaced, while 2-hydroxy-butanoic acid was replaced with tartaric acid. Other quantity of undefined acids were represented as levulinic acid, also for compensating the number of non-hydroxylated carbons present in the simulated mixture, subtracted in part by tartaric acid representation.

Table 3: Spent black Kraft liquor chemical model. Part A is reprinted from [2]. *Xylonic acid was actually added as D-xylono-1,4-lactone.

Part A		Part B			
Real liquor composition		Liquor modeling		Representative solution	
Chemical - all acids	$m_{real,prod}$ /kg	Model chemicals	$m_{model,prod}$ /kg	ω	$m_{chemical}$ /g
glycolic	25	glycolic	25	0.12	2.16
lactic	25	lactic	25	0.12	2.16
3,4-dideoxypentonic	10	/	/	/	/
glucoisosaccarinic	35	gluconic	35	0.17	3.1
2-hydroxybutanoic	60	tartaric	60	0.3	5.4
3-deoxypentonic	10	/	/	/	/
Xyloisosaccarinic	25	xylonic*	25	0.12	2.16
Others	40	levulinic	40	0.17	3.1
Total	230	Total	210	1	18.05

An Agilent 7890A gaschromatograph was used for the analysis of the gas phase products, equipped with Poraplot Q and Molecular Sieves columns in series, allowing the quantification of CO_2, H_2, CH_4, CO and polar/non-polar light gases.

HPLC was used for the analysis of the liquid phase (Jasco), equipped with a SepaChrom Benson Polymeric BP-OA BL0053 (2000-0) PS-DVB sulphonated gel column and a BP-OA BL0059 pre-column, both immersed in an isothermal bath at 45.6°C. The system was equipped with a UV-Vis detector and a Refractive Index one. This allowed to identify the reactants conversion, but only some of the possible intermediates were identified and calibrated, given that a full speciation is almost impossible for this application.

Therefore, a COD/TOC method was employed to determine the total organic carbon present at the beginning and at the end of the tests, further allowing to check the mass balances. 5 mL of solution

taken at times 0 and 5 h were placed in clean round bottomed glass vacutainers. 5 mL of 0.178 M (≈1.1 N) $K_2Cr_2O_7$ solution and 5.5 mL of concentrated H_2SO_4 (96%) were added. In a third vacutainer only $K_2Cr_2O_7$ solution and sulfuric acid were added to compose the blank inorganic solution. All vacutainers were then closed and put in a digestion oil bath, placed on a big heating-stirring plate, at 130°C for 30 min. The stirring was set to 400 rpm. Just after few minutes, one can see that the colour of the sample solutions shifts from orange to bottle green, indicating reduction from Cr^{6+} to Cr^{3+}, meanwhile the blank one remains orange. After 30 min, the samples were cooled and their content was quantitatively transferred into 3 different 200 ml volumetric flasks, which were brought to volume. The solutions were analysed twice in a Perkin Elmer Lambda 35 double ray UV-Vis Spectrophotometer at 605 nm.

A Shimadzu TOC-L CSH/CPH was also used to test 50 µl aliquots of a 1:20 diluted sample prepared from the solution spilled from the reactor. This was injected onto a platinum catalyst at 680 °C in an oxygen rich atmosphere. Ultra-high purity air carrier gas transports the produced CO_2 through a moisture trap and halide scrubbers to remove water vapor and halides from the gas stream, before it reaches the detector, to avoid possible interferences. A non-dispersive infrared (NDIR) detector is then used to measure CO_2 generated concentration.

3. Results and discussion

3.1 Catalysts characterisation

The DR-UV-Vis recorded spectra reporting %R values were elaborated as Kubelka-Munk patterns and further in form of Tauc plots. The calculated band gaps are reported in Table 4. The P25 TiO_2 photocatalyst absorbs in the UV portion of the spectrum, only. A bathochromic shift can be noticed for all the metal loaded samples, increasing with metal loading and metal dispersion, since the spectra of decorated catalysts were shifted to higher wavelengths with respect to bare P25. The reasons of

this effect can be attributed to sub-band-gap energetic levels insertion at metal-TiO_2 heterojunctions. Furthermore, plasmonic contributions are also evident in the visible region.

Table 4: Optical, structural and textural properties of the prepared catalysts. D = crystal size from Scherrer equation; BET SSA = BET Specific Surface Area.

Catalyst	Eg (eV)	Anatase%	Rutile %	D Anatase (nm)	D Rutile (nm)	BET SSA (m^2/g)	Pore volume (cm^3/g)
P25	3.41	78	22	15	75	45.5	0.21
0.36 wt%Au/P25	3.27	86	14	18.3	65.7	47.3	0.396
0.36 wt%Pt/P25	3.12	86	14	18.8	65.1	55.1	0.472
1 wt%Au/P25	3.11	/	/	/	/	/	/
1 wt%Pt/P25	3.07	/	/	/	/	/	/
1 wt%Au_6Pt_4/P25	2.85	81	19	19.8	82.2	53.3	0.486
1 wt%Au_8Pt_2/P25	2.88	80	20	20.2	87.1	51.9	0.485

X-rays diffractograms were collected for all the catalysts and reported in Fig. 1.

Figure 1: XRPD diffractograms of the studied catalysts. Phase attribution as: # anatase (JCPDS card 21-1272); * rutile (JCPDS card 21-1276). a) P25; b) 1 wt%Au_6Pt_4/P25; c) 1 wt%Au_8Pt_2/P25; d) 0.36 wt%Pt/P25; e) 0.36 wt%Au/P25.

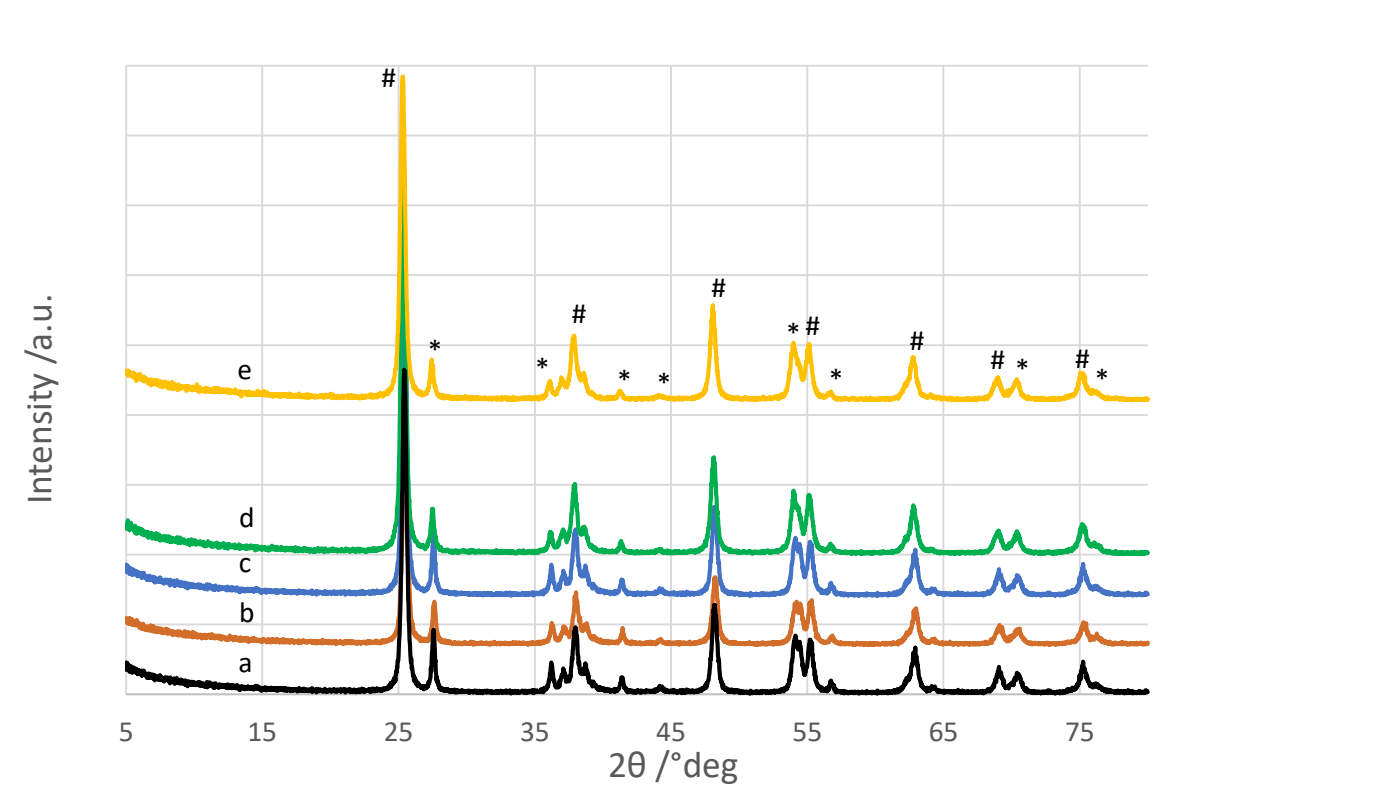

The P25 sample was constituted of a mixture of anatase and rutile, the former predominant (Table 4) and constituted by smaller crystals than rutile. No specific reflections relative to the metals were present, as expected due to their low amount and high dispersion.

Interestingly, the crystal sizes remained quite similar for all the samples, indicating that the thermal treatment for the monometallic samples did not affect the crystal phases. Indeed, no significant structural differences were found considering reduction under milder or harsher conditions.

N_2 adsorption/desorption isotherms of all the catalysts were classified as type IV isotherms, representing N_2 probe adsorption on both mesoporosity of limited extent and open surfaces. The raw data were elaborated through the Brunauer Emmet and Teller (BET) algorithm and the results are reported in Table 4. External surface area and BET surface area were comparable for the metal-loaded samples and of the same order of magnitude of the bare P25 sample. Porosity is essentially due to

nanoparticles agglomerates, since the flame synthesis used for the aeroxide titania leads to dense nanoparticles. Total pore volume increased almost doubling for the metal containing samples coherently with the formation of agglomerates after impregnation or precipitation.

3.2 Effect of metal loading

The results of all the tests are reported in Table 5, which reports the conversion of the reactant (when it is a single component) and/or the conversion of the organic carbon as calculated comparing the carbon content of the liquid and gas phase at times 0 and 5 h. Furthermore, the productivity of the gas phase products and of arabinose (as the only liquid phase product) are reported. All the tests were checked for mass balance, which resulted close to 100% for all the tests if not else specified.

Table 5: Activity testing results. HS = hole scavenger; GLU = GLUcose; TA = Tartaric Acid; BKL = Black Kraft Liquor; SSL = Spent Sulfite Liquor.

Catalyst	HS	pH	Conversion HS %	TOC Conv. %	Arabinose	H_2	CO_2	CO	C_2H_4	CH_4	C_2H_6
P25	GLU	3.5	0.3	0.7	9.9	92.6	171.7	27.32	0	0	0
	GLU	5	2.8	/	17.4	155.2	232.2	94.9	65.7	0	0
	GLU	7	7.2	/	34.6	571.1	139.1	346.1	159	1.41	0
	GLU	12.5	/	/	/	0	52.2	44.7	0	9.6	0
0.36 wt%Au/P25	GLU	7	8.9	/	68.5	3225.3	685.8	532.6	89.3	7.2	371.8
0.36 wt%Pt/P25	GLU	7	13.2	/	97.2	3549.1	830.3	438.4	/	39.8	376.8
1 wt%Au/P25	GLU	7	4.7	0.3	27.1	721.1	129.9	117.7	/	6.2	71
1 wt%Pt/P25	GLU	7	7.5	1.4	65.7	1522.3	382	289	50.8	27.7	409.5
1 wt%Au_6Pt_4/P25	GLU	7	15.2	/	109.35	4124	810.2	422.9	159.1	/	59.4
1 wt%Au_8Pt_2/P25	GLU	7	11.4	/	85.4	3679.2	741.3	396.7	98.8	1.2	158.4
P25	TA	2-3	39.7	12.2	/	324.9	5992.9	415.6	/	412.5	2669.9
1 wt%Au_6Pt_4/P25	Sim. BKL	2-3	/	21.7	/	170.4	2659.2	275.6	135.2	507.3	3449.6
0.36 wt%Pt/P25	Sim. BKL	2-3	/	15.8	/	480.6	3517.6	303.6	129.1	511.6	4650.6
0.36 wt%Pt/P25	Sim. SSL	3	/	9.7	/	98.4	419.9	/	/	476.1	/

The results in terms of glucose conversion, H_2 productivity, by-product productivities and time profile

of H_2 evolution (total moles of H_2 produced from t_0 to t_n) of the various tests are summarized in Table 5 and Fig. 2.

Figure 2: Comparison of a) glucose conversion and H_2 productivity, b) productivity to other gas phase compounds and c) H_2 evolution *vs*. time for the mono-metallic co-catalysts.

a)

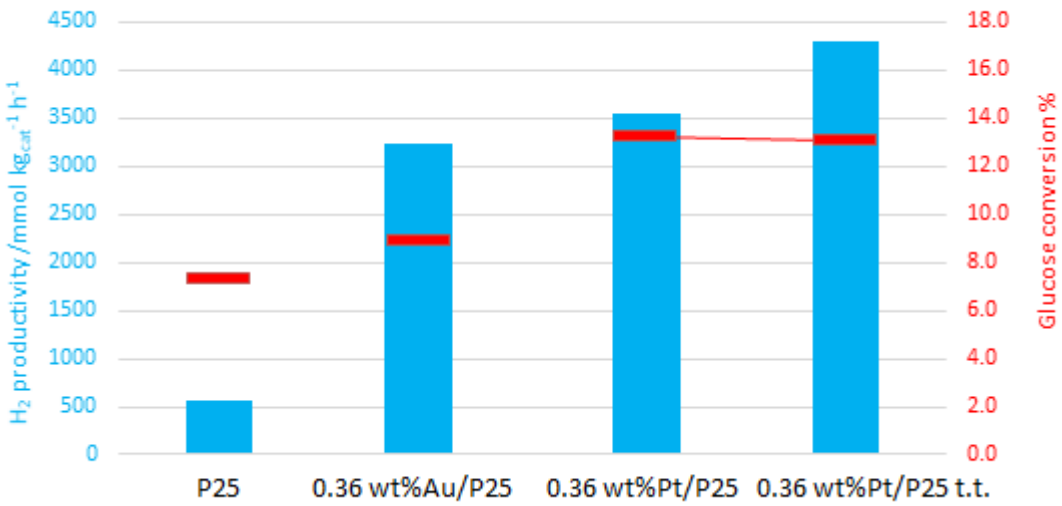

b)

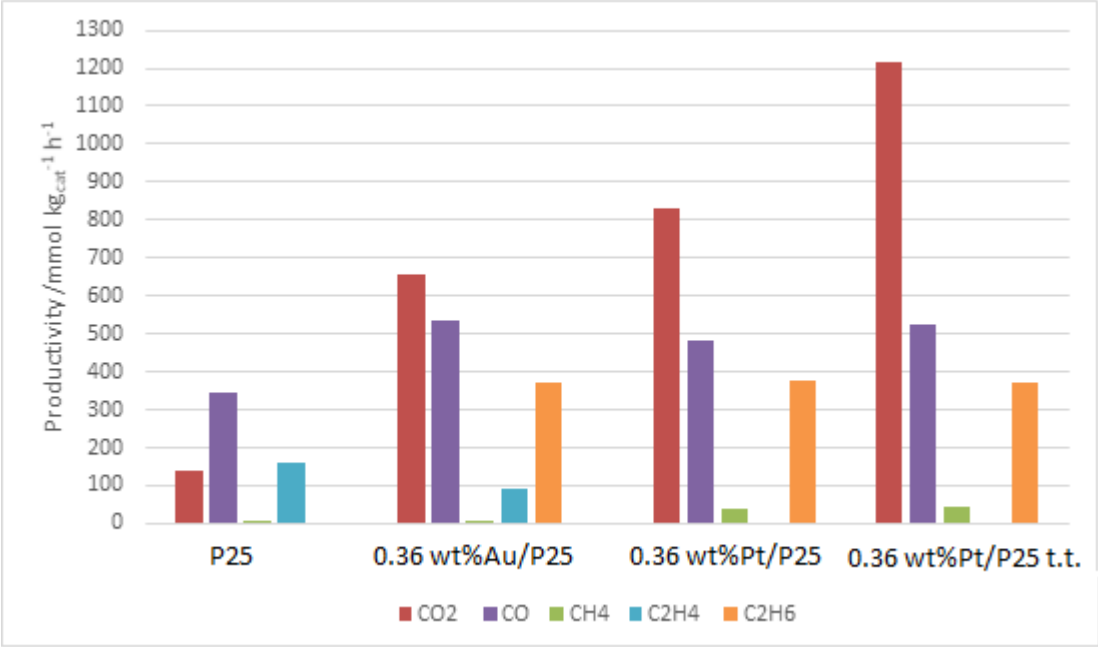

c)

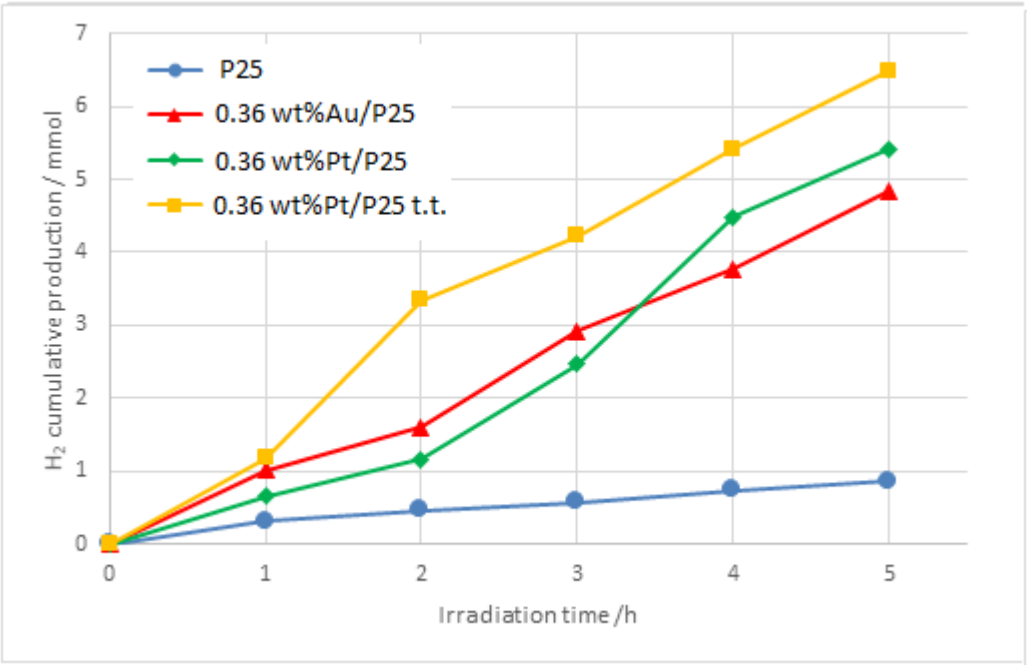

Glucose conversion increased with respect to bare P25 after loading 0.36 wt% of Au and mostly of Pt, which showed the best co-catalyst. Hydrogen productivity was boosted even more with co-catalyst addition, more than 5 times the one of the P25 benchmark for all the samples tested, with a maximum of 3549 mmol kg_{cat}^{-1} h^{-1} for 0.36 wt%Pt/P25 (ca. 7 times the one of P25). Higher metal loading up to

1 wt% was however detrimental, leading to a decrease of both HS conversion and H_2 productivity, very likely due to lower metal dispersion and to a shielding effect by the metal, inhibiting light absorption by the semiconductor. Further thermal treatment of the Pt-loaded sample was attempted by doubling the reduction time. This further treatment was intended to further reduce titania at 700°C, promoting the formation of oxygen vacancies. This should increase the light harvesting by the semiconductor, which consequent improvement of the irradiation efficiency. After prolonged reduction, the products distribution and conversion of glucose remained almost unaffected, with some increase of hydrogen productivity, only.

Time profiles of hydrogen evolution have a linear evolution with time, suggesting that no significant catalyst poisoning or deactivation is evident and that nearly constant hydrogen production rate can be expected.

The main by-products were CO_2 and CO, whose sum was substantially similar for all the samples. Other gas-phase byproducts were ethane, ethylene and methane (minor), with productivities comparable among all the catalysts.

Textural properties are very similar between the various samples, justifying the similar performance but confining the main difference in the potentials and Fermi level positioning of the different samples.

Pt loaded catalyst showed the highest productivity among the other single metal loaded catalysts, due both to the H_2 evolution overpotential, which is lower for Pt than for Au [25] and in terms of work function. Higher thermodynamic driving force for electron transfer across metal/semiconductor junction is expected for Pt. The higher the work function, the more efficient the surface electron trapping effect, by virtue of the strong difference in contact potentials that anyhow is generated in the heterojunctions, both for nanometric and not nanometric surface decorated semiconductors.

However, Schottky barriers formation (with both higher heights and penetration depths as higher the work function differences are) cannot be fully invoked to explain the data, due to the effect of the nanometer size. The effects of efficient charge separation could be linked to kinetic reasons. A

possible explanation may be the following: metals high reactivity (surely also linked to a lower H_2 evolution overpotential) would lead to such a sudden electron spilling from the metal islands as not to significantly change their Fermi level under illumination. In this way, the driving force for holes entry in the metal would remain low. If we consider the practical implications of the Fermi level splitting under irradiation, semiconductor hole quasi-Fermi level should be stabilized around the values of mixed potential experienced by the semiconductor, or around its more positive E_{rev} (vs. SHE) components. In any case, Pt Fermi level would be at higher energy for the holes. Au Fermi level would be at holes higher energy if the semiconductor holes quasi-Fermi level would be around the Open Circuit Potential (OCP) values (4.58 eV in our case), while at lower energy if the latter was around the reversible O_2 evolution potential (ca. 5.10-5.30 eV, values around 5.76 eV can be obtained with O_2 saturation). All this can be valid if the conditions of actual metal Fermi level pinning occur, therefore if semiconductor/metal junction surface states can allow preferred electrons transit, and their reactive spilling on metal islands is favored.

This reasoning works well in the Pt case, but for Au can present criticalities. It does not fit the possibility of this latter to work as preferential hole trap and electron injector by Localised Surface Plasmon Resonance (LSPR) effects. Apart from giving metal NPs the possibility to trap surface holes while draining electrons in semiconductor's conduction band, LSPR polarizes the reactant molecules in the fluid and increases the adsorption to the metal surface, also heating up the local environment, so reactant mass transfer is improved.

The simultaneous addition of Au and Pt co-catalysts was also explored through a sol-immobilisation technique, in order to achieve the highest possible dispersion, as recently demonstrated for a different application [23,26]. In this way we were able to keep ca. 0.4 wt% of Pt, added with Au 0.6 wt%, to check any cooperative effect. We also tuned the ratio between Pt and Au as 0.2/0.8 wt%, keeping fixed the total amount of metals to 1 wt%.

Figure 3: Performance of bi-metallic co-catalysts: a) cumulative H_2 evolution *vs*. time and b) productivity of other gas phase compounds.

a)

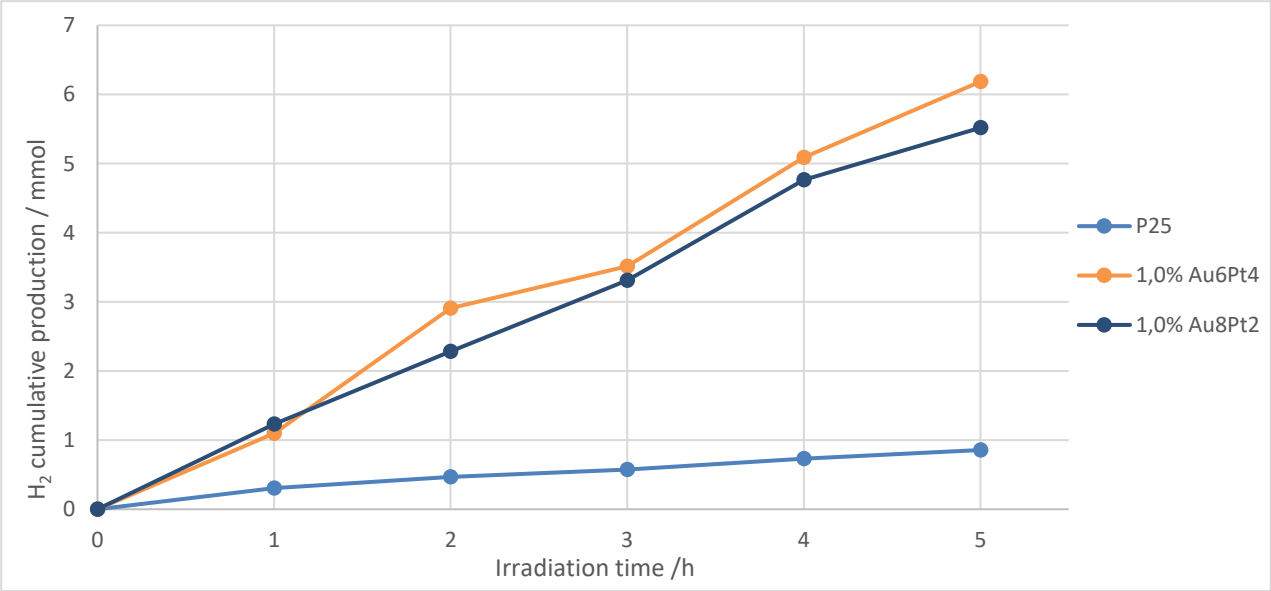

b)

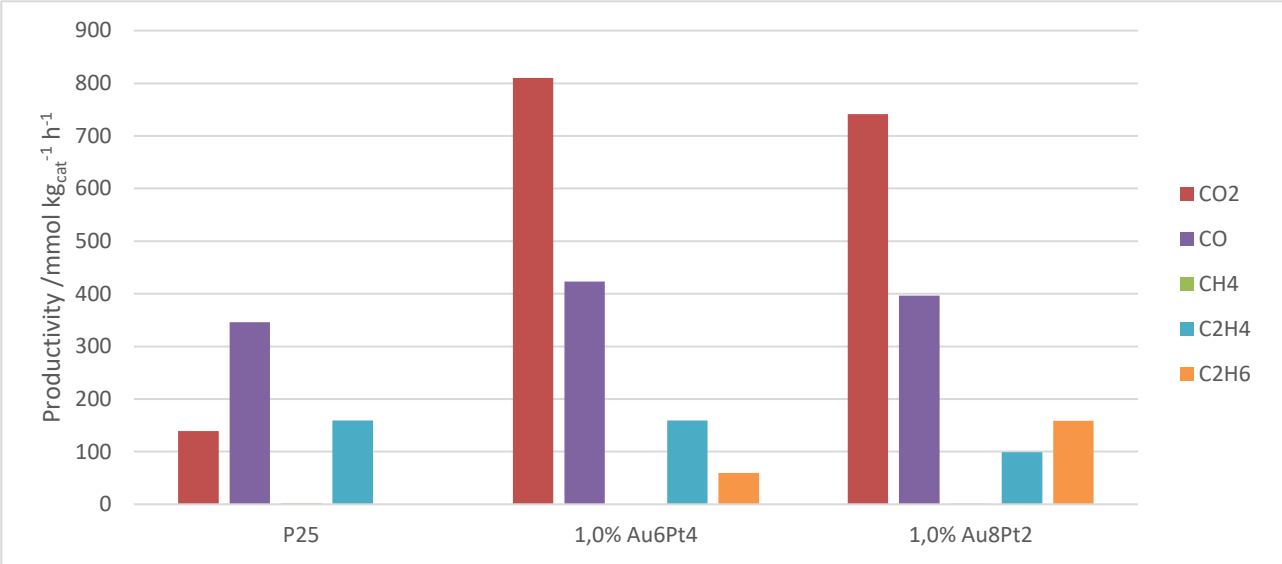

Glucose conversion was slightly higher than for the mono-metallic Pt (15.2% vs. 13.2%) for 1.0 wt%Au_6Pt_4/P25, showing a possible cooperative effect of Au for Pt, while it decreased for 1.0 wt%Au_8Pt_2/P25 catalyst (11.4%), likely due to the halved Pt content. Furthermore, hydrogen productivity reached higher values, 7 and 6 times higher than the one experienced by P25 (4124 mmol kg_{cat}^{-1} h_{irr}^{-1} and 3679 mmol kg_{cat}^{-1} h_{irr}^{-1} for 1.0 wt%Au_6Pt_4/P25 and 1.0 wt%Au_8Pt_2/P25 respectively). A higher Pt content could improve the synergy among Pt effective electron surface trapping and gold related LSPR effects of induced periodic excitation of semiconductor holes and electrons. A periodic draining of gold photoexcited electrons to P25 can happen, while holes are retrieved across the heterojunction. It might be hypothesized that the sol immobilization preparative methods created metal/semiconductor junction surface states suitable to promote these cooperative effects. This is not obvious. Some work on non-nanometric TiO_2 shows how gold particles can act as mere surface hole traps in which their Fermi level is not pinned [5,27]. In this case the possible accumulation of holes would lead it to more negative energy quotes (towards more positive potentials) promoting it as recombination site, as a greater driving force would be created for the access of surface electrons. This effect is greatly amplified by the related Schottky barriers at the junction, in our case considered ineffective, but it can exist regardless of them.

The cumulative H_2 production also showed a linear behaviour without any evidence of deactivation.

The main by-products were CO_2 and CO, while low quantity of CH_4 and ethane were produced. CO productivities are almost equal for both bimetallic catalysts (ca. 400 mmol kg_{cat}^{-1} h_{irr}^{-1}) while CO_2 one follows the same trend of H_2 productivity.

Both catalysts are almost equal from the textural point of view, so, also in this case, it can be assumed that the performances are substantially determined by the nature of metal/semiconductor junctions and their intrinsic disposition to promote the reactions involved in the photoreforming process.

As comparison, TiO_2 catalysts promoted with C quantum dots returned H_2 productivity of 1.42 mmol kg_{cat}^{-1} h_{irr}^{-1} [28]. Pt was also considered as co-catalyst in addition with reduced graphene oxide, tested under UVB irradiation. Under such conditions, H_2 productivity up to ca. 20 mol kg_{cat}^{-1} h_{irr}^{-1} was observed loading 1 wt% Pt at pH 7, against a 1 mol kg_{cat}^{-1} h_{irr}^{-1} attained with bare P25 in the same conditions but using glycerol as hole scavenger, a much easily reformable compound [29]. Pt/TiO_2 photocatalysts proved effective also for the photoreforming of aqueous solutions of cellulose, leading to ca. 0.16-0.20 mol kg_{cat}^{-1} h_{irr}^{-1} hydrogen productivity, with decreasing performance while increasing Pt loading [30].

As for the formation of intermediates and for the general reaction mechanism, a recent investigation highlights the decomposition pathway for cellulose. Oxygen insertion at C1 position is considered the first step, followed by the elimination reaction, which oxidatively cleaves the β-1,4-glycosidic bond with formation of gluconic acid and glucose. The latter is hen oxidized into gluconic acid which is subsequently oxidized or decarboxylated into glucaric acid or arabinose [31]. This frame of reactions confirms arabinose as primary intermediate pf the photoreforming of glucose.

3.3 pH effect on reactivity

The pH substantially influences the nature of the surface states and the catalyst pH_{PZC}, i.e. the pH value at which the surface reaches zero charge. Usually, the activity tests have been carried out at the naturally established pH, which is nearly neutral when glucose is used as HS. However, the pulping residues are composed of different substances, possibly lowering the pH of the solution. Therefore,

to decouple the effect of HS composition and of pH, activity testing at different pH was carried out with glucose as HS. The point of zero charge of the bare P25 catalyst was previously determined as 6-6.5 [32,33] (Table 5 and Fig. 4). Both acid and alkaline pH dramatically depress productivities and conversion, especially at pH = 12.5, where no H_2 production at all has been detected for the whole test. The conversion of glucose at pH 12.5 test was not calculated because it was not possible to identify the glucose peak in the HPLC chromatogram, crowded by many unidentified peaks. Such sample appeared after 5 h irradiation as a brown solution with a caramel scent.

Figure 4: a) Glucose conversion and products distribution after 5 h irradiation with P25 catalyst at different pH; b) hydrogen generation vs. time of irradiation

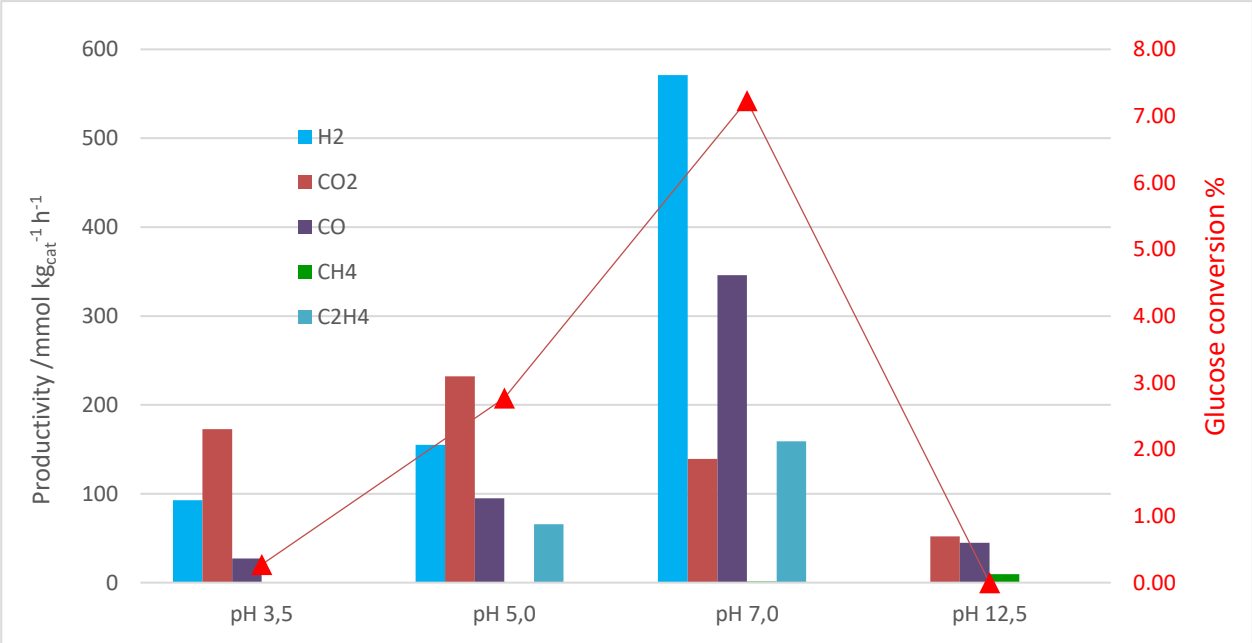

b)

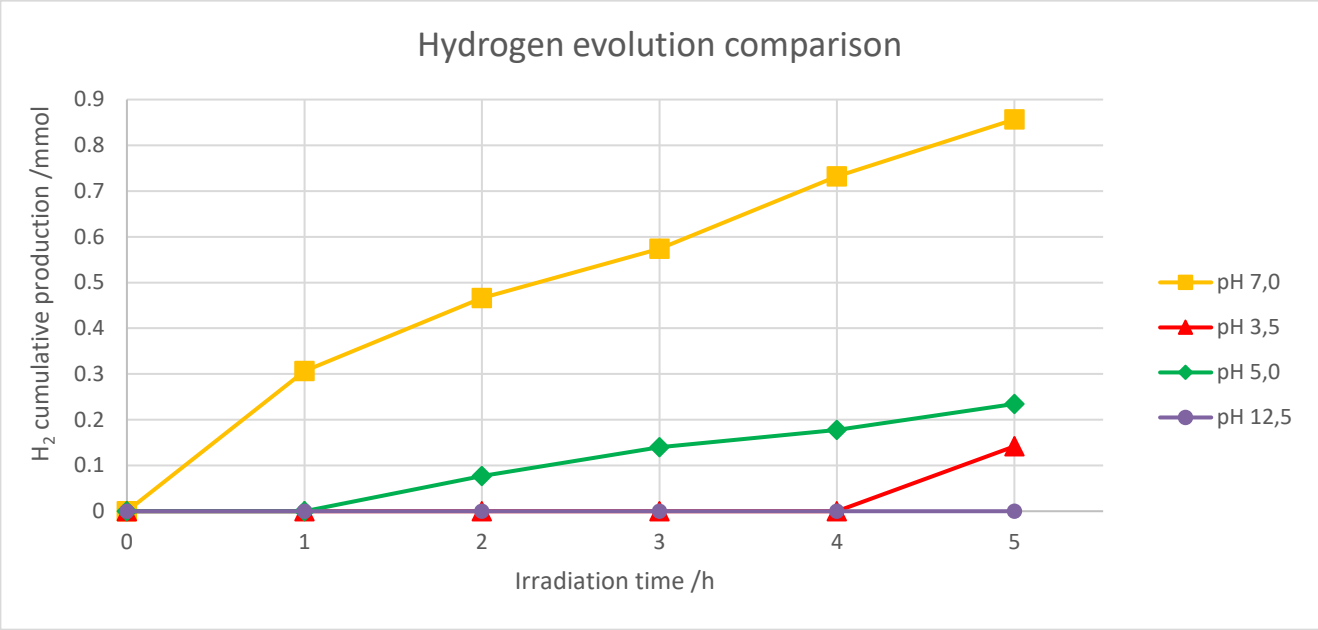

As for the evolution of products during time, a steady H_2 productivity was observed, regularly and almost linearly increasing with irradiation time.

By comparing the productivities of H_2 and of the sum of CO and CO_2, a similar trend with pH can be observed passing through a maximum between pH 5 and 7. However, while at these two pH the ratio between H_2 and ($CO+CO_2$) is ca. 1, fairly well representing the stoichiometric proportion in the glucose molecule, at acid and basic pH the activity seems mainly oxidative, with evolution of CO_x but limited production of H_2. Arabinose production follows the same trend of H_2 in liquid phase. However, many other byproducts are formed in the liquid, impossible to singly identify and quantify, but roughly estimated by considering the carbon content of the solution after irradiation. The conversion of organic compounds calculated by COD-TOC analysis reveals systematically a much lower conversion than that calculated from the bare hole scavenger. Prolonged irradiation time is thus needed to fully convert all the organic intermediates after glucose completely converts.

Other products in gas phase were very poor with P25 catalyst, leading to the production of some ethylene only at neutral pH.

TiO_2 band edge are unpinned to pH changes, since its surface groups that determine their energetic quote are influenced by pH, as all oxides surface $M\text{-}OH^-$ and $(M)_2 – OH^+$ groups. However, it has

been demonstrated that they exhibit a Nernstian behavior with respect to pH changes, varying their quasi-Fermi levels with similar slope of E_{H^+/H_2} and E_{O_2/H_2O}:

$$E^{rev}_{H^+/H_2} = E^0_{H^+/H_2} - kpH = -0{,}0592\frac{mV}{dec}\,pH \quad and \quad E^{q-Fl}_{CB} = -0{,}17 - 0{,}054\frac{mV}{dec}\,pH$$

so variations in differences among quasi - Fermi level of electrons of the semiconductor (identifying the conduction band edge) and the one of the couple H^+/H_2 are not responsible for lower reduction rates. Of course, the potential that we define and measure to quote the Fermi level of the semiconductor after equilibration (OCP) is a mixed potential, determined by all the E^0, or better E_{rev} level of the redox couples of the electrolytes, but the causes of its variation can be identified only by the variation of E_{H^+/H_2} term and eventually E_{O_2/H_2O} term if oxygen is dissolved, since the other E_{rev} most frequently established are independent from pH variations. The situation would have been really different and complicated in the case of loaded catalyst, since charge carrier access to some types of surface state such as metal and oxide NPs deposited may be precluded. That's why this investigation is more significant with bare semiconductors.

By virtue of these electrolyte potentials of redox couple pinning toward pH variation, relative energetic positions among quasi-Fermi levels and E_{rev} may be rationalised according to the nanometric modeling of energy levels in the following way.

Acid pH: quasi fermi level of electrons is shifted in a Nernstian way toward more negative energies of the absolute scale so less negative corresponding E_{rev} value, thus toward less energetic state for electrons. In this way it gets closer to the energetic quotes of organic oxidations. At the same time, holes quasi fermi level should follow the shifting of the electron one, increasing its "energetic difference" and therefore potential energy gradient with those fermi levels of organic species in solution. Their oxidation should be favored. However, not such a great increase of gaseous oxidation products has been highlighted.

Basic pH: quasi fermi level of electrons is shifted in a Nernstian way toward less negative energies of the absolute scale, so more negative corresponding E_{rev} value, thus toward higher energetic state for electrons. In this way it gets further to the energetic quotes of organic oxidations. Hole quasi fermi

level should follow this upward shifting, getting “energetically closer” to those organic solution fermi levels, decreasing the potential energy gradient among them. In fact, productivities of the gaseous oxidation products are very limited at pH 12.5.

These considerations are made only from a thermodynamic point of view. Further kinetic consideration can be made trying to explain those results. It has been stated that valence band edge should follow the shifts of the conduction band one. This is valid for non-nanometric photocatalysts. In our case, discussions are still open in literature regarding the relationship among the actual position of the valence band edge, the related hole quasi-Fermi level position and their relative pinning with respect to the displacements of the conduction band edge due to chemical changes of the electrolytes [3].

Great availability of H^+ ions should prompt reductions at acid pH, but H_2 productivities are actually much lower than at neutral pH. This might be due to electrostatic repulsion among the largely positively charged catalyst surface and H^+ ions, since pH 3 << pH_{PZC} of TiO_2: the majority of surface groups are in their acid form [13].

Reasons beyond low productivity of gaseous oxidation products are difficult to find in literature. They might be linked to complex concatenated kinetics among glucose oxidation pathways and its acid HMF driven oligomerization. HMF can be obtained by dehydration of glucose in acid environment. It can occur both in the electrolyte bulk and on pH acid made catalyst surface [19]. Maybe hole scavenging properties of such obtained oligomers could be different from glucose from the adsorption point of view.

Moreover, the concatenation among degradative pathways of oligomers may difficultly lead to products easy to degrade towards gaseous products, or anyway can decrease the number of carbons that can be oxidized according to proposed pathways. It can be suggested that the difficulty of producing carboxyl groups that can be oxidized according to radical decarboxylations or photo-Kolbe electro-oxidations considerably limits the degradation pathway towards simpler products in the liquid and gaseous phase. Moreover, a balance between glucose oligomerization and oligomer

depolymerization can also occur due to electrolyte acidity. Beyond this, it should not be forgotten that the conversion of glucose determined by HPLC analysis is close to 0. This cannot be explained by this kind of reasoning.

As far as we know, no empiric detailed studies about glucose adsorption on bare photocatalyst at different pH can be found in literature. However, some computational studies based on DFT calculations can be found for glucose adsorption on determined face of single crystals [34]. These studies foresee an adsorption of glucose through its hydroxyl moieties to Ti ions with a coordination vacancy, so as to arrange oxygen against the metal atom and the H atom towards the O bridge between two nearby metal atoms. Such models do not foresee the presence of chemically adsorbed water molecules. One recent proven hypothesis of oxidation mechanism can help in this kind of reasoning [35]. They show that glucose anomeric -OH group and its vicinal one can directly catch surface metal atom after having displaced chemisorbed water. Then they undergo hole injection by Ti surface groups. The final result of hole scavenging is the conversion of a hemiacetal carbon to a formate ester grafted group. This formate ester intermediate can present a radical localized on another carbon of the chain, which can undergo current doubling phenomena to effectively complete the process and leaving the active site free. This peculiar rearrangement and subsequent formate hydrolysis can be considered as the slowest step of the reaction, leading to the blocking of the surface state and increasing electron hole recombination. Acid hydrolysis of the grafted intermediate has been proven ineffective, while basic one more efficient, even if conducted at pH < pKa of glucose. In neutral condition, the so called light driven hydrolysis was invoked as mechanism of formate hydrolysis, managing to keep a balance between grafting of formate intermediates and their desorption as formic acid and C-1 saccharide [35].

At basic pH, the low concentration of free H^+ ions and glucose deprotonation can be indicated as causes of the total absence of H_2 evolution. According to [13] a surface negative charge effect can be again invoked. The pKa of glucose is ca. 12.3. When the solution pH is lower than glucose pK_a, its most stable molecular forms are not charged. As the solution pH becomes higher than dissolved

glucose pKa, it will be deprotonated, forming an enendiolate anion, negatively charged. TiO_2 surface under such pH environment is mainly negatively charged too, because pH > pH_{PZC}. The electrostatic repulsion between them will inhibit glucose adsorption and consequently, all photocatalytic related performances.

At basic pH glucose can also undergo multiple homogeneous reactions, as described in references [36,37]. These reactions, with complex kinetics, lead to the formation of products with a higher molecular weight which, by adsorbing on the catalyst, could also be oxidized, but with much longer and more complex mechanisms than that hypothesized for glucose, which can link up with inverse aldolizations and oligomerizations promoted by the basic environment in the homogeneous phase.

It can be assumed that this concatenation can in any case lead to the oxidative insertion of -OH· radicals or to the formation of carbon radicals by extraction of -H·, however, they decrease from time to time the number of extractable hydrogens and the lack of sufficient quantities of easily oxidizable aldehyde groups and which can lead to de-carboxylations can imply a further delay in the formation of formic acid and in the routing towards degradative pathways that involve simpler compounds as products, such as the ones found in gas phase. This delay might imply not so quick hole scavenging. The possible oxidations, even of aldehyde groups, can however be linked to the other reactions occurring in this environment.

3.4 Photoreforming of simulated pulp industry processed liquors

Tartaric acid was selected as model molecule representative of the whole mixture of acids, deriving from pulp processing. The best catalysts identified during glucose photoreforming were employed and the naturally established solution pH was not changed.

Tartaric acid conversion reached ca. 40%, more than 5 times higher than that of glucose (7.2%). Other marked differences concern the productivity of CO_2 and ethane, which were so high as to define them as main products, e.g. CO_2 productivity of ca. 6000 mmol kg_{cat}^{-1} h_{irr}^{-1} has been achieved. Ethane productivity was also outstanding (2670 mmol kg_{cat}^{-1} h_{irr}^{-1}). The overall conversion of organic content

was higher for tartaric acid (12.2% vs. 0.7% of glucose), indicating faster degradation also of the intermediates of oxidation.

Figure 5: Comparison of hole scavenger conversion and productivity. HS concentration = 5 g/L.

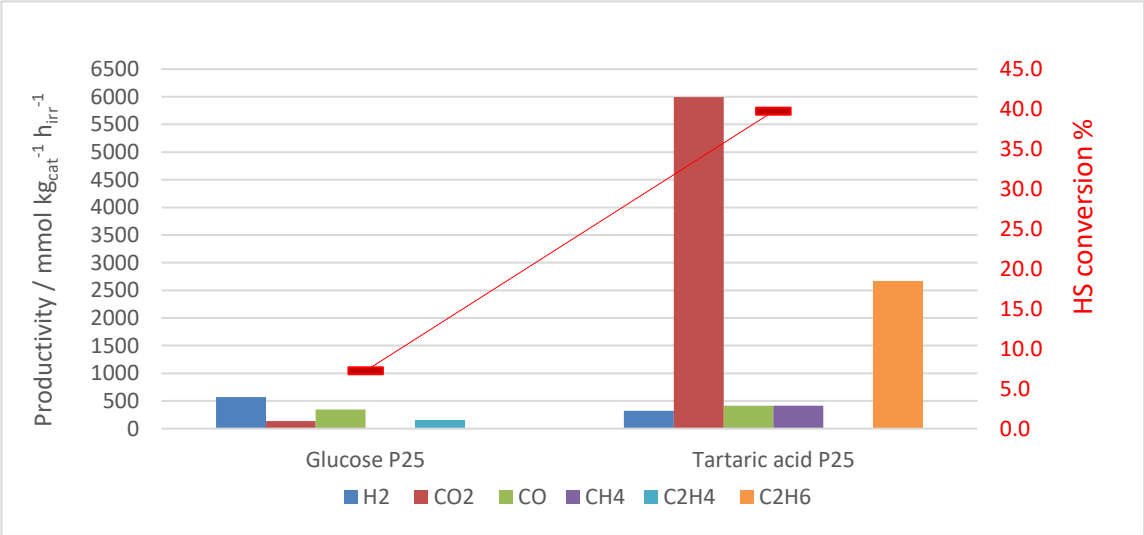

On one hand such a different reactivity may be due to a different adsorption mechanism of tartaric acid on the surface states in which the holes are stored. The oxidation mechanism may also be simpler than glucose, implying fewer potentially blocking steps for the active site and favoured by the presence of highly oxidised functions. The low H_2 evolution rate can be explained considering that the decarboxylation of the two extreme carboxylic groups can occur fast (high CO_2 productivity) leaving an ethandiol intermediate that can dehydroxylate leaving to a stable ethane residual, accumulating in the gas phase without further conversion.

The two simulated pulp industry waste liquors were then tested, increasing the concentration of HS to 15 g/L to be more adherent to real cases. This may imply reactivity problems the regarding photoreforming of the simulated sulfite spent liquor (which is rich of carbohydrates). Indeed, a previous work from our research team [19] showed that too high concentration, e.g. > 6-8 g/L, glucose molecules crowded the catalyst surface so that only a very little part of it underwent all the degradation steps, since statistically its rarer for an intermediate already desorbed to be adsorbed

again and proceed along the degradation pathway: glucose molecules displace them with an higher frequency. Moreover, according to the recently reported degradation mechanism by Sanwald et al. [35] both too high degree of glucose adsorption and fast intermediate displacing may increase the number of blocked surface states to a level such as to decrease its hole scavenging properties: if many surface states are involved in the hypothesized current doubling phenomena and even more in redox-neutral photoinduced hydrolysis (both slower than a hole trapping in the time scale) photogenerated holes following the ongoing surface reaction find fewer free sites to be trapped, increasing the possibility of recombining with electrons. Furthermore, humins formation [19] favored by an acid environment, can dramatically prompt these phenomena. For this reason, only one test was performed on sulfite spent liquor with 0.36 wt%Pt/P25.

The carbon conversion to volatile products χ_{TOC}, H_2 productivity, by-product productivities and time profile of H_2 and ethane evolution are reported in Fig. 6.

Figure 6: Comparison of a) Kraft black liquors conversion and productivity, b) Sulphite liquors conversion and productivity, c) time dependent products evolution for Kraft black liquors.

a)

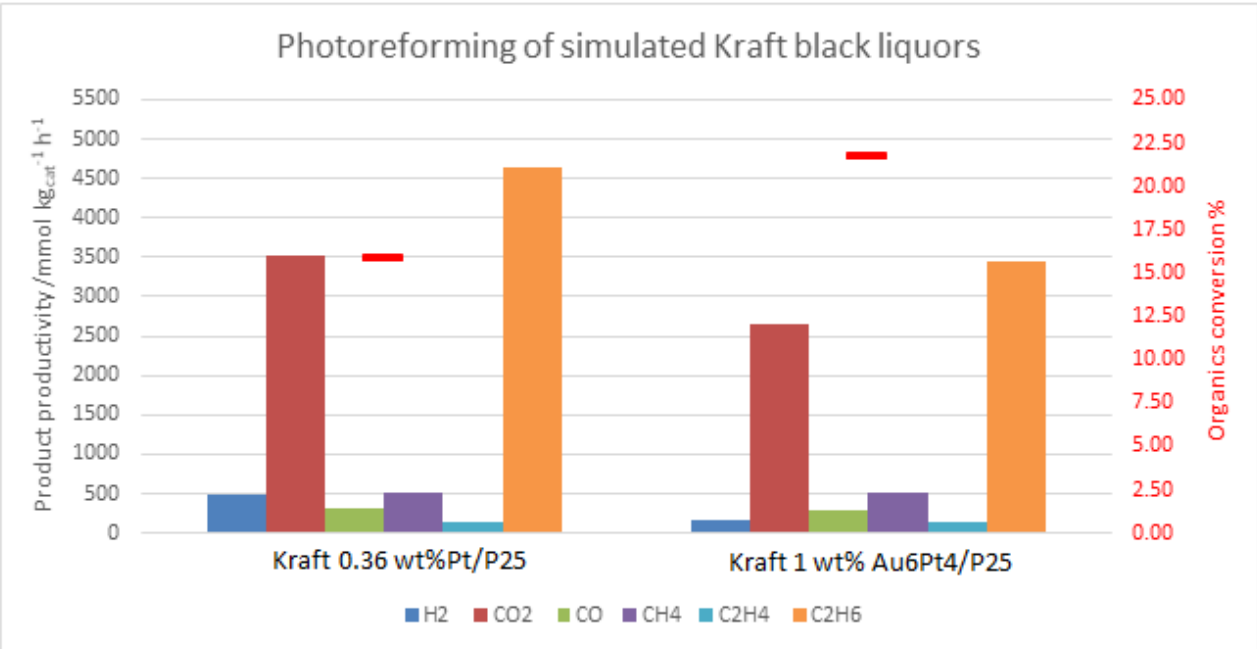

b)

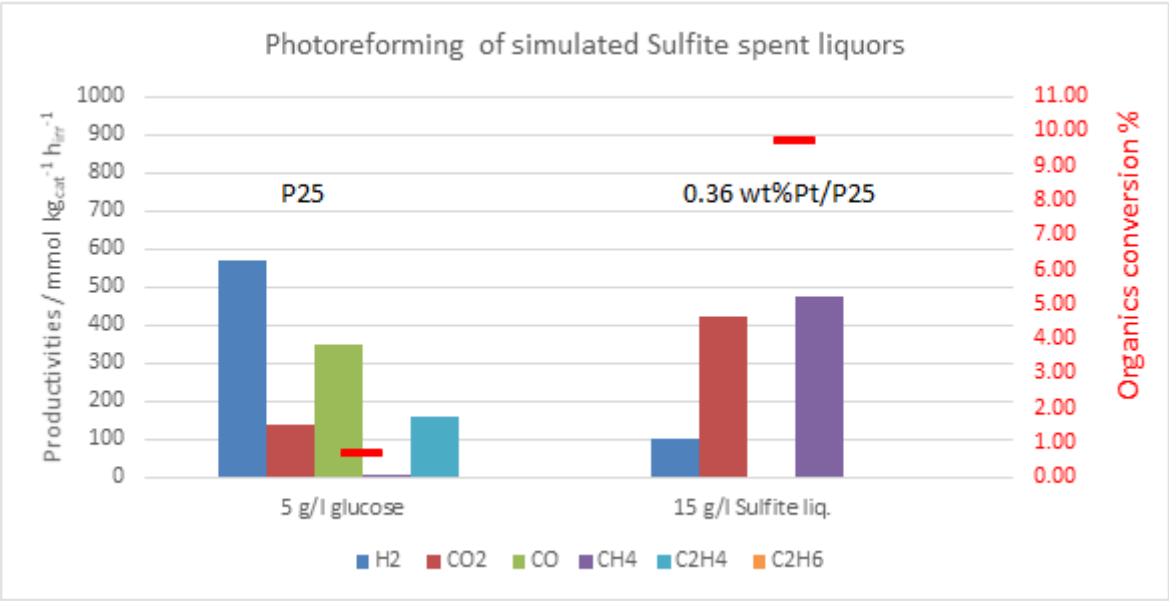

c)

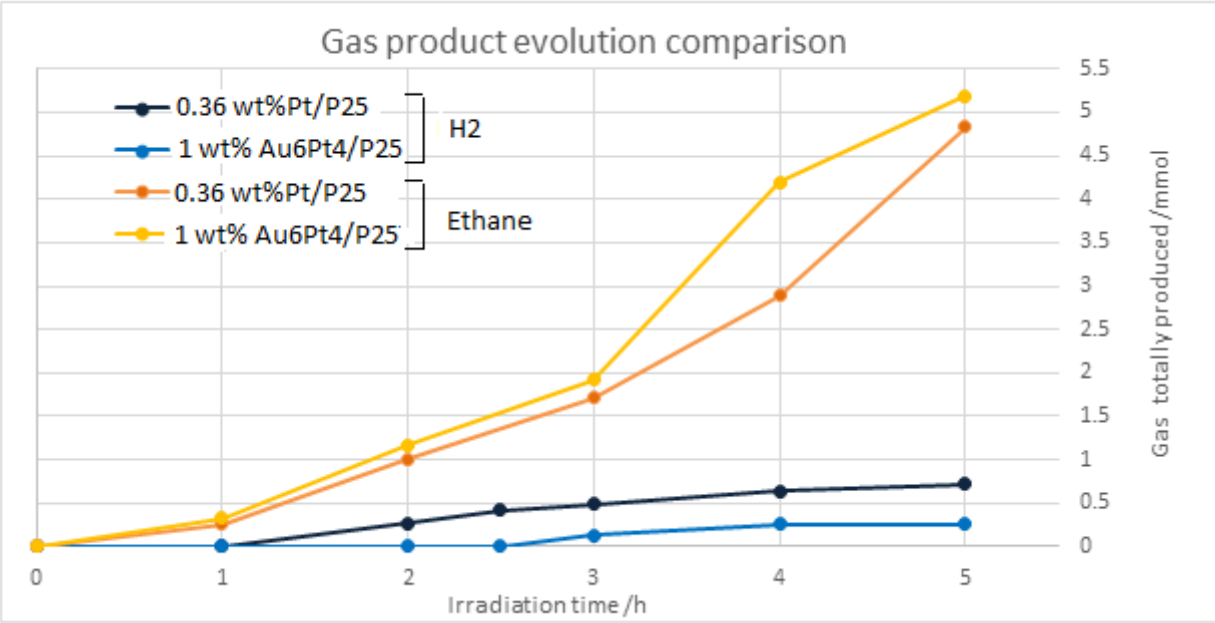

The main products observed during the photoreforming of the Kraft black liquor were CO_2 and ethane, both evolved with much higher productivities than the average CO_2 and H_2 productivities found for all tests of glucose photoreforming. Ethane productivity of 0.36 wt%Pt/P25 and 1.0 wt%Au_6Pt_4/P25 were 4651 and 3450 mmol kg_{cat}^{-1} h^{-1}, respectively, comparable to the H_2 productivities obtained for glucose photoreforming. Other products productivities were lower than 500 mmol kg_{cat}^{-1} h^{-1}.

Total organics conversions were at least 10 times higher than those obtained in glucose

photoreforming tests, suggesting greater ease of HS oxidation and a tendency in their possible degradation mechanisms to promote pathways that produce gaseous compounds. A reasonable mechanism could be an -OH· mediated one, partly similar to that hypothesized by Gomathisakar [11]. However, the dominant presence of ethane as in TA photoreforming strongly suggests the decarboxylating-dehydroxylating mechanism described above for such model molecule. This is in line with the average composition described in Table 3, which indicates as main components, besides lignin, hydroxycarboxylic acids. Some authors also suggested that methane and ethane can be produced from formic and oxalic acids dehydration and hydrogenation [38]. The acid pH and higher actual total HS concentration seem not to hinder reactivity, in line with the hypothesis of hydroxy-acids simpler degradation mechanism and at difference with the more complex multistep glucose photoreforming.

The time profiles of products evolution were curvilinear both for H_2 and ethane, but with different concavity, flattening out for hydrogen, increasing with time for the hydrocarbon. In light of valorising the spent pulping wastewaters in form of gaseous fuels this is anyway an important result.

The results for the photoreforming of the simulated sulphite processed liquors were less satisfactory. Organics conversion was again much higher than in the case of glucose, likely thanks to the presence of simpler substrates, but half the one obtained for the Kraft spent liquor. Also, H_2 was a minor product with respect to glucose photoreforming (98 mmol kg_{cat}^{-1} h^{-1}). Only CO_2 and CH_4 were detected as other products, the latter with a productivity of ca. 500 mmol kg_{cat}^{-1} h^{-1}. They may derive from acetic acid and gluconic acid degradation. Possibly, in this case oligomeric humins by-products can have formed and deposed over the catalyst, as pointed out by references [19,39], since the mass balance closed to only 90%.

4. Conclusions

The photoreforming of glucose, tartaric acid and simulated pulp processing waste liquors has been explored as a mean to produce H_2 and other gaseous fuels through the valorisation of waste industrial

solutions. Noble metal loaded P25 based catalyst (0.36 wt%Pt/P25 and 1.0 wt%Au_xPt_y/P25) were the most active catalysts tested both in terms of glucose conversion (higher than 10% after 5 h irradiation) and H_2 productivity (they all exhibit productivities higher than 2.8 mol kg_{cat}^{-1} h_{irr}^{-1}). The best one among them was 1.0 wt%Au_6Pt_4/P25, returning > 4 mol kg_{cat}^{-1} h_{irr}^{-1}). This result is of the same order of magnitude of the best productivity published until now regarding glucose photoreforming for metal loaded catalysts (ca. 5.7 mol kg_{cat}^{-1} h_{irr}^{-1} [13]).

Generally speaking, all tests display low glucose conversion and an even lower carbon conversion to gaseous products. A devoted kinetic debottlenecking study should be conducted on the theme, starting from the work of Sanwald et al. [35].

Moreover, it can be stated that catalytic activity is almost totally defined by the intrinsic nature of the co-catalyst loaded than by a mutual effect of co-catalyst loading and textural properties variations.

Tartaric acid, as a model for carboxylic acid products, returned higher conversion than glucose, but the reaction mechanism led to the formation of CO_2 and ethane as main products. This may not be a problem if the scope of the reaction should be the valorisation of a waste substrate in form of a gaseous fuel mixture. In line with this, Black Kraft liquor testing showed carbon conversion to gaseous products higher than in the case of glucose photoreforming, suggesting an easier mechanism, predominantly involving the hydroxycarboxylic acids components.

On the contrary, the sulfite spent liquor led to higher conversion of organics than glucose, even though halved with respect to the Kraft one, producing mainly methane as valorisable fuel.

A discussion on the effect of band potentials variation with pH allowed to conclude that the best operating conditions are neutral pH, which may impose the necessity of pH adjustment in case of acidic pulping spent solutions.

In all cases the photoreforming reaction demonstrated feasible for simple substrates, with high hydrogen productivity. With complex mixtures photoreforming is more suitable for the abatement of the COD of the wastewater than for hydrogen production and may be considered as a valuable option to produce hydrocarbon containing gaseous fuels.

References

[1] Roudier S, Kourti I, Delgado Sancho L, Rodrigo Gonzalo M, Suhr M, Giner Santonja G, et al. Best Available Techniques (BAT) Reference Document for the Production of Pulp, Paper and Board. JRC Science and Policy Reports; 2015. https://doi.org/10.2791/370629.

[2] Sjostrom E. Wood Chemistry, Fundamentals and Applications. Second Ed. 1993.

[3] Krishnan R. Fundamentals of Semiconductor Electrochemistry and Photoelectrochemistry. Encycl. Electrochem., vol. 1, Wiley; 2002. https://doi.org/10.1002/9783527610426.bard060001.

[4] Linsebigler AL, Lu G, Yates JT. Photocatalysis on TiO2Surfaces: Principles, Mechanisms, and Selected Results. Chem Rev 1995;95:735–58. https://doi.org/10.1016/S0035-9203(29)90032-8.

[5] Nakato Y, Tsubomura H. Structures and functions of thin metal layers on semiconductor electrodes. J Photochem 1985;29:257–66. https://doi.org/10.1016/0047-2670(85)87076-3.

[6] Ueda K, Nakato Y, Suzuki N, Tsubomura H. Silicon Electrodes Coated with Extremely Small Platinum Islands for Efficient Solar Energy Conversion. J Electrochem Soc 1989;136:2280–5. https://doi.org/10.1149/1.2097300.

[7] Matsumura M, Uchihara T, Hanafusa K, Tsubomura H. Interfacial Band Structure of Platinum-Loaded CdS Powder and Its Correlation with the Photocatalytic Activity. J Electrochem Soc 1989;136:1704–9. https://doi.org/10.1149/1.2096996.

[8] Wang H, Zhang L, Chen Z, Hu J, Li S, Wang Z, et al. Semiconductor heterojunction photocatalysts: Design, construction, and photocatalytic performances. Chem Soc Rev 2014;43:5234–44. https://doi.org/10.1039/c4cs00126e.

[9] Kelly JJ, Vanmaekelbergh D. Charge carrier dynamics in nanoporous photoelectrodes. Electrochim Acta 1998;43:2773–80. https://doi.org/10.1016/S0013-4686(98)00018-8.

[10] De Jongh PE, Vanmaekelbergh D. Trap-limited electronic transport in assemblies of nanometer-size TiO2 particles. Phys Rev Lett 1996;77:3427–30. https://doi.org/10.1103/PhysRevLett.77.3427.

[11] Gomathisankar P, Kawamura T, Katsumata H, Suzuki T, Kaneco S. Photocatalytic hydrogen production from aqueous methanol solution using titanium dioxide with the aid of simultaneous metal deposition. Energy Sources, Part A Recover Util Environ Eff 2016;38:110–6. https://doi.org/10.1080/15567036.2012.750400.

[12] Huang Y-B, Fu Y. Hydrolysis of cellulose to glucose by solid acid catalysts. Green Chem 2013;15:1095–111. https://doi.org/10.1039/c3gc40136g.

[13] Fu X, Long J, Wang X, Leung D, Ding Z, Wu L, et al. Photocatalytic reforming of biomass: A systematic study of hydrogen evolution from glucose solution. Int J Hydrogen Energy 2008;33:6484–91. https://doi.org/10.1016/j.ijhydene.2008.07.068.

[14] Christoforidis KC, Fornasiero P. Photocatalytic hydrogen production: a rift into the future energy supply. ChemCatChem 2017;9:1523–44. https://doi.org/10.1002/cctc.201601659.

[15] Bahadori E, Ramis G, Zanardo D, Menegazzo F, Signoretto M, Gazzoli D, et al. Photoreforming of glucose over CuO/TiO2. Catalysts 2020;10:477. https://doi.org/10.3390/catal10050477.

[16] Ramis G, Bahadori E, Rossetti I. Design of efficient photocatalytic processes for the production of hydrogen from biomass derived substrates. Int J H2 Energy 2021;46:12105–16. https://doi.org/https://doi.org/10.1016/j.ijhydene.2020.02.192.

[17] Ramis G, Bahadori E, Rossetti I. Photoreactors design for hydrogen production. Chem Eng Trans 2019;74:481–6. https://doi.org/10.3303/CET1974081.

[18] Sellerio F, Rossetti I, Ramis G. Photoreforming of carbohydrates: catalysts screening. University of Milan, 2018.

[19] Villa A, Rossetti I, Ramis G. Optimization of the reaction conditions for the photoreforming of carbohydrates. University of Milan, 2018.

[20] Villa A, Ferri D, Campisi S, Chan-Thaw CE, Lu Y, Kröcher O, et al. Operando Attenuated Total Reflectance FTIR Spectroscopy: Studies on the Different Selectivity Observed in Benzyl Alcohol Oxidation. ChemCatChem 2015;7:2534–41. https://doi.org/10.1002/cctc.201500432.

[21] Wang D, Villa A, Porta F, Su D, Prati L. Single-phase bimetallic system for the selective oxidation of glycerol to glycerate. Chem Commun 2006:1956–8. https://doi.org/10.1039/b518069d.

[22] Rossetti I, Ramis G. Catalytic, photocatalytic, and electrocatalytic processes for the valorization of CO<inf>2</inf>. Catalysts 2019;9. https://doi.org/10.3390/catal9090765.

[23] Bahadori E, Tripodi A, Villa A, Pirola C, Prati L, Ramis G, et al. High pressure CO 2 photoreduction using Au/TiO 2 : unravelling the effect of co-catalysts and of titania polymorphs. Catal Sci Technol 2019;9:2253–65. https://doi.org/10.1039/C9CY00286C.

[24] Galli F, Compagnoni M, Vitali D, Pirola C, Bianchi CL, Villa A, et al. CO2 photoreduction at high pressure to both gas and liquid products over titanium dioxide. Appl Catal B Environ 2017;200:386–91. https://doi.org/10.1016/j.apcatb.2016.07.038.

[25] Lee SK, Mills A. Platinum and palladium in semiconductor photocatalytic systems. Platin Met Rev 2003;47:61–72. https://doi.org/10.2307/3456057.

[26] Bahadori E, Tripodi A, Villa A, Pirola C, Prati L, Ramis G, et al. High Pressure Photoreduction of CO2: Effect of Catalyst Formulation, Hole Scavenger Addition and Operating Conditions. Catalysts 2018;8:430. https://doi.org/10.3390/catal8100430.

[27] Nakato Y, Tsubomura H. The Photoelectrochemical Behavior of an n-TiO 2 Electrode Coated with a Thin Metal Film, as Revealed by Measurements of the Potential of the Metal Film. Isr J Chem 1982;22:180–3. https://doi.org/10.1002/ijch.198200035.

[28] Zhao H, Yu X, Li CF, Yu W, Wang A, Hu ZY, et al. Carbon quantum dots modified TiO2 composites for hydrogen production and selective glucose photoreforming. J Energy Chem 2022;64:201–8. https://doi.org/10.1016/j.jechem.2021.04.033.

[29] Mohan P S, Purkait MK, Chang CT. Experimental evaluation of Pt/TiO2/rGO as an efficient HER catalyst via artificial photosynthesis under UVB & visible irradiation. Int J Hydrogen Energy 2020;45:17174–90. https://doi.org/10.1016/j.ijhydene.2020.04.072.

[30] Lan L, Daly H, Jiao Y, Yan Y, Hardacre C, Fan X. Comparative study of the effect of TiO2 support composition and Pt loading on the performance of Pt/TiO2 photocatalysts for catalytic photoreforming of cellulose. Int J Hydrogen Energy 2021;46:31054–66. https://doi.org/10.1016/j.ijhydene.2021.06.043.

[31] Zhao H, Li CF, Yu X, Zhong N, Hu ZY, Li Y, et al. Mechanistic understanding of cellulose β-1,4-glycosidic cleavage via photocatalysis. Appl Catal B Environ 2022;302:1–8. https://doi.org/10.1016/j.apcatb.2021.120872.

[32] Bahadori E, Conte F, Tripodi A, Ramis G, Rossetti I. Photocatalytic Selective Oxidation of Ammonia in a Semi-Batch Reactor: Unravelling the Effect of Reaction Conditions and Metal Co-Catalysts. Catalysts 2021;11:209. https://doi.org/10.3390/catal11020209.

[33] Bahadori E, Tripodi A, Ramis G, Rossetti I. Semi-Batch Photocatalytic Reduction of Nitrates: Role of Process Conditions and Co-Catalysts. ChemCatChem 2019;11:4642–52. https://doi.org/10.1002/cctc.201900890.

[34] Balducci G. The adsorption of glucose at the surface of anatase : A computational study. Chem Phys Lett 2010;494:54–9. https://doi.org/10.1016/j.cplett.2010.05.068.

[35] Sanwald KE, Berto TF, Eisenreich W, Jentys A, Gutiérrez OY, Lercher JA. Overcoming the Rate-Limiting Reaction during Photoreforming of Sugar Aldoses for H 2 -Generation. ACS Catal 2017;7:3236–44. https://doi.org/10.1021/acscatal.7b00508.

[36] de Bruijn JM, Kieboom APG, van Bekkum H. Alkaline Degradation of Monosaccharides. Starch/Staerke 1987;39:23–8. https://doi.org/10.1002/star.19870390107.

[37] de Bruijn JM, Kieboom APG, van Bekkum H. Alkaline degradation of monosaccharides III. Influence of reaction parameters upon the final product composition. Recl Des Trav Chim Des Pays-Bas 1986;105:176–83. https://doi.org/10.1002/recl.19861050603.

[38] Zhao H, Liu P, Wu X, Wang A, Zheng D, Wang S, et al. Plasmon enhanced glucose photoreforming for arabinose and gas fuel co-production over 3DOM TiO2-Au. Appl Catal B Environ 2021;291. https://doi.org/10.1016/j.apcatb.2021.120055.

[39] Bahadori E, Ramis G, Zanardo D, Menegazzo F, Signoretto M, Gazzoli D, et al. Photoreforming of Glucose over CuO/TiO2. Catalysis 2020;10:1–20. https://doi.org/10.3390/catal10050477.